



Experimental and Numerical Investigation of Air Flow Motion in Cylinder of Heavy Duty Diesel Engines

C. Demirkesen^{1†}, U. Colak², I. H. Savci¹ and H. B. Zeren¹

¹ Ford Otomotiv Sanayi A.Ş., İstanbul, Sancaktepe, 34885, Turkey

² Department of Energy Science and Technology, Istanbul Technical University, İstanbul, Maslak, 34669, Turkey

†Corresponding Author Email: cdemirke@ford.com.tr

(Received April 9, 2019; accepted July 29, 2019)

ABSTRACT

In recent years, numerical simulations have become key tool for diesel engine combustion system development due to the requirement of the shorter development duration for the improved performance and better emission levels. In this study, an approach, which integrates numerical and experimental methods in order to characterize the flow field in diesel engine cylinder, is presented. The steady-flow port bench testing, PIV (Particle Image Velocimetry) measurements and numerical simulation methods are used to determine the flow behavior inside the cylinder. Numerical simulation method is validated by using experimental results in terms of mass flow rate and swirl ratio in cylinder. Mass flow rate values predicted within 5 percent error and swirl ratio values predicted within 10 percent error. This proves the viability of numerical method as an important alternative to port bench measurements. In addition to that, cylinder-to-cylinder variation and effects of surface roughness are investigated by swirl ratio measurements and optical diagnostic. Results showed that surface quality and manufacturing problems have significant effects on the swirl ratio in cylinder.

Keywords: CFD; Swirl ratio; Port design; Flow test bench; Compression.

NOMENCLATURE

CFD	computational fluid dynamics	ρ_s	density for isentropic process
C_μ	turbulence model constant	\dot{m}	mass flow rate
D	swirl ratio	$\dot{m}_{mea.}$	measured mass flow rate
K	ratio of specific heats	$\dot{m}_{theor.}$	theoretical mass Flow Rate
k	turbulent kinetic energy	c_s	velocity for isentropic process
M	torque	μ	dynamic viscosity
PIV	particle image velocimetry	μ'	dilatational viscosity
P_1	upstream pressure	ε	turbulent dissipation
P_2	downstream pressure	τ	Reynolds stress
R	gas constant	β	turbulence model constant
S	source term	η_0	turbulence model constant
SCR	selective catalytic reduction		
ρ_{cyl}	density in cylinder		

1. INTRODUCTION

Diesel engines have become main power source for heavy duty, light duty, and passenger vehicles in recent years. Diesel engines are higher torque and thermal efficiency than gasoline engines (Heywood 1998). However, despite all these advantages of diesel engines, harmful exhaust gases from the engine limits the combustion efficiency (EUROPARL, 2009). Emission standards for diesel

engines have become very strict in European regulations. European Union regulations introduce a significant reduction of nitrogen oxides (NOx) emission from Euro 5 to Euro 6 for diesel engines (Krishnan, 2005).

Two main approaches are mainly used to reduce emission level. The first method relies on the after treatment system to reduce the emission. Diesel engines requires exhaust after treatment system since diesel combustion is not sufficient to reduce NOx

and soot for Euro6 (Gan *et al.*, 2016). Selective Catalytic Reduction (SCR) is designed to efficiently reduce NOx emissions from the combustion system. The SCR is an emission reduction system that contains injector, catalyst, the urea water solution and urea tank and control system (Sun *et al.*, 1996; Weltens *et al.*, 1993; Steger, 1995). The second method is to optimize the combustion process, which reduces the emission level without advanced after treatment system (Hirata *et al.*, 2005).

Optimizing the diesel combustion is critical step during the design phase but phenomenological physics of the combustion is challenging. To enhance phenomenological physics of the combustion, complex flow structure should be designed and manipulated (Kamimoto and Kobayashi, 1991). As diesel engines have undergone a step development curve in recent years, it is appropriate to reassess current practices for the characterization of in-cylinder flow during combustion system development, using state of the art numerical and experimental techniques.

Swirl is angular momentum given to air during suction stroke to ensure optimum air-to-fuel mixture to achieve engine performance in terms of power emissions. Swirl is amplified at the end of the compression stroke by forcing the air towards the cylinder axis into the bowl-in-piston combustion chamber. The nature of the swirling flow in an actual engine is extremely difficult to determine (Stone and Ladommatos, 1992).

Flow structures are mostly generated during the admission stroke and evolved under the influence of volume reduction during the compression stroke. Combustion characteristics of the modern diesel engine relies on the application of charge air motion around the center axis of the combustion chamber (Roy and Penven, 1998).

Although engine manufacturers have different design philosophies, adapting the level of swirl generated during the admission stroke to obtain the required air-to-fuel mixture and combustion quality is one of the important strategies in diesel engine development activities. Performing such fine optimization requires a detailed knowledge and understanding of the underlying flow features (Tippelmann, 1977 & Uzman *et al.*, 1983).

Considering the intake port generates the swirl behavior in-cylinder, its flow performance has significant influence on engine power, fuel economy, and exhaust emissions. Swirling flow is mainly used to get adequate fuel-air mixing rates and this determines the combustion efficiency. So that, measurement of the air motion becomes increasingly important due to exhaust emissions as well (Han *et al.*, 2007).

The main method that has a wide spread usage to measure the global swirl level generated by the intake port is steady state flow port bench testing. In such experimental set-up, the head mounted on top of an open-end cylinder. A constant pressure difference across this set-up induces a steady flow of air. The mass flow rate that is achieved gives an

indication of the cylinder head's efficiency. Torque meter is used to measure the intensity of the swirling air flow that passes through the cylinder for several fixed positions of the intake valve. The measurement results are used to calculate a global non dimensional swirl number for which various mathematical definitions exist.

It is well known that in diesel engine, swirl is needed for proper mixing of fuel and air and for the higher combustion efficiency. Moreover, the efficiency of diesel engine can be increased also by increasing the burn rate of fuel. This can be achieved by two ways; either by designing the combustion chamber in order to reduce the interaction between the flame and the chamber surface or by designing the intake system that imparts swirling motion to intake charge. The intake port for 4-valve system and flow through intake port can be analyzed with CFD (Computational Fluid Dynamics) in suction condition at different lift conditions but in this paper flow patterns, streamlines and velocity vectors observed at full lift (Hoffmann *et al.*, 1995).

As it was reported in the literature, the swirl in diesel engines is an important parameter that affects the mixing rate of air and fuel, heat release rate, emissions, and overall engine performance (Costa *et al.*, 2014). It is also observed that there is an optimum level of swirl for particular combustion chamber geometry. If required, the swirl level could increase with an appropriate combustion chamber design. It was observed that an increase in the swirl affects the fuel-air mixture (Kim *et al.*, 2014).

One of the other important parameters, which can affect the swirl behavior inside the cylinder is surface quality and manufacturing processes. Since it is well-known that solid surfaces, irrespective of their method of formation, contain irregularities or deviations from the prescribed geometrical form (Whitehouse, 1994; Bhushan, 1996; 1999a, b; Thomas, 1999). The surfaces contain irregularities of various orders ranging from shape deviations to irregularities of the order of interatomic distances. No machining method, however precise, can produce a flat surface on conventional materials. Even the smoothest surfaces, such as those obtained by cleavage of some crystals, contain irregularities, the heights of which exceed the interatomic distances. For technological applications, both macro- and micro/nanotopography of the surfaces (surface texture) are important (Bhushan, 1999a, b). This study verified that surface quality of the engine head has an effective role on the swirl ratio parameter. Manufacturing errors have a role of %40 on the flow performance of the cylinder head (Bhushan, 1999a, b).

Many research groups investigated the effects of the swirl on the combustion, engine performance and emission levels. Numerical methods and their capabilities to predict the swirl ratio are studied in different studies, as well. However, any research group has not proposed a complete port design methodology, yet. The main motivation of this study is to investigate the important parameters, which can affect the swirl ratio/behavior in-cylinder and to

propose a complete port design methodology by including a plastic prototyping approach, various measurement techniques, numerical methods, manufacturing problems and surface roughness effects.

The objective of the present study is to develop comprehensive numerical and experimental port development methodology, which can predict swirl ratio for the virtual signoff. For this purposes, a steady-state numerical model with adaptive mesh refinement technique is developed in Converge commercial CFD software. Then this numerical model is compared and validated with steady state port bench measurements. Optical swirl test bench is built to correlate swirl center to understand flow behavior. At the same time further experimental studies show that manufacturing variations such as surface roughness and valve tilt have significant effect on the swirl ratio. Therefore hybrid port development methodology is proposed to capture significant noise factor.

2. EXPERIMENTAL INVESTIGATION

2.1 Steady Flow Test Bench

In the present study, a steady flow test bench is used to measure the swirl ratio. Steady flow testing is a simplification of the real flow problem, which is the unsteady in-cylinder flow in a running engine due to the piston movement and valve movements. The reason of considering the steady flow testing is a result of the complexity to measure actual flow behavior during the engine operation.

Since the steady flow conditions are considered, piston is not included in the test set-up. Instead of piston, a honeycomb is mounted which does not have any motion. Airflow obtained by a blower with a constant pressure difference.

After mounting the cylinder head to the bench, all the test cycle runs automatically. For each valve lift starting from 1 mm up to maximum valve lift for the considered engine, swirl ratio is measured. Position sensors control the valve lift arrangement as seen in the Fig. 1. In the end, the output of the measurements is a swirl ratio profile over the valve lift.

In the test bench utilized in this study, swirl ratio measured indirectly by using the angular momentum of the flow. Since the airflow has an angular momentum due to the shape of the intake port before entering the combustion chamber. The tangential component of the airflow is damped with a honeycomb geometry in the bench and due to the conservation of the momentum; transformed to a force on the honeycomb walls and measured with a torque meter located under the honeycomb as shown below in the Fig. 2.

By using the torque value, the dimensionless swirl ratio is calculated with the equation below:

$$D = \frac{M \times R_{Cyl} \times \rho_{Cyl}}{\dot{m}^2} \quad (1)$$

Furthermore, the second important parameter for this

kind of a measurement is the flow coefficient, which is calculated by

$$\alpha_k = \frac{\dot{m}_{measured}}{\dot{m}_{theor.}} \quad (2)$$

The $\dot{m}_{theor.}$ with

$$\dot{m}_{theor.} = A_k \times \rho_s \times C_s \quad (3)$$

Where A_k is the engine cylinder section area, ρ_s is the isentropic density and C_s is the isentropic velocity.

$$C_s = \sqrt{\frac{2 \times K}{K-1} R \times T \times \left(1 - \left(\frac{p_2}{p_1} \right)^{\frac{K-1}{K}} \right)} \quad (4)$$

$$\rho_s = \frac{p_1}{R \times T} \times \left(\frac{p_2}{p_1} \right)^{\frac{1}{K}} \quad (5)$$

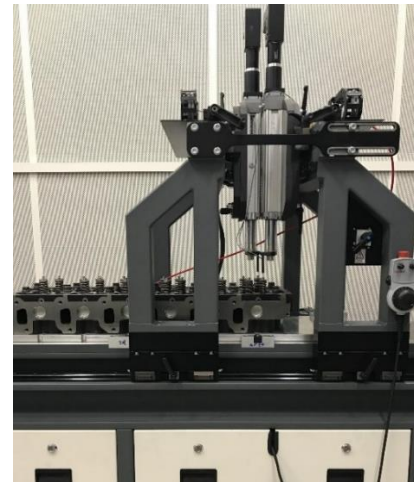


Fig. 1. Steady flow test bench.

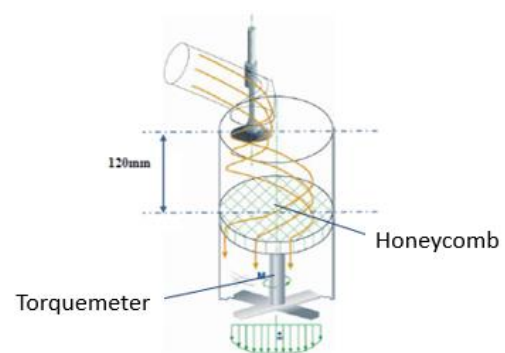


Fig. 2. Details of measurement system.

2.2 Optical Diagnostics: Particle Image Velocimetry

The steady flow rig is a simplification for the transient flow phenomenon inside the combustion chamber. There are a few measurement techniques to observe the data for the transient flow behavior

during the engine operation. Particle image velocimetry (PIV) has a wide usage for the research projects. In recent years, OEM companies started using PIV systems for the engine development activities, as well. PIV is a non-intrusive technique, but test engine must be equipped accordingly to supply an optical access to the flow.

Due to the aim of this study, PIV module of the flow bench is used for steady flow measurements. Engine cylinder manufactured with a transparent material to be able to access to flow optically.

Fig. 3 shows the details of the PIV system used in this study.

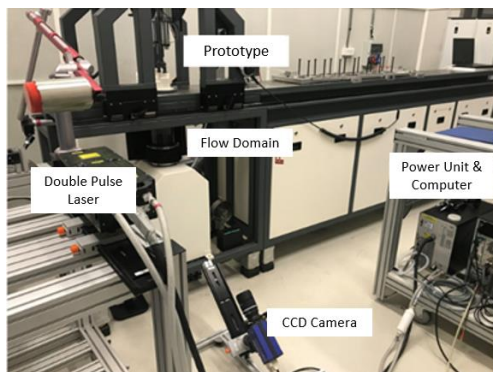


Fig. 3. PIV system.

Laser sheet is located 125 mm below the cylinder head. Laser system is equipped with a robot arm to reach cylinder area.

Particle size and particle density are crucial parameters to observe enough resolution to understand the flow behavior and the circulation areas in cylinder. In the literature, it is stated that particle size and the density should be chosen according to flow conditions. Due to the different refractive index of liquid and gases, the particle illumination is easier for the gas flows. Therefore, bigger particle sizes like 10-1000 μm for the liquid flow conditions and smaller particle size like 0.5-10 μm for the gas flow conditions should be chosen (Haktan *et al.*, 2012).

In the present study, particle size is chosen accordingly and used as 8 μm . To observe the sufficient information for the flow circulation zones on the considered section, medium particle density is used like the Fig. 4(b).

A CCD (Couple-Charged Device) camera is used for the photographing. Instead of instantaneous pictures, average of last 100 pictures is used for the investigations and comparison with the CFD results. Since RANS (Reynolds Averaged Navier-Stokes) model is used as explained in the following sections and average flow is the consideration in this study due to the large-scale swirl motion.

2.3 Surface Roughness Effect

There are a number of parameters affecting the swirl ratio. The intake port design, manufacturing

tolerances, and errors have crucial influence on the flow behavior and the swirl ratio.

In the present study, to assess the measurement repeatability and the accuracy, three different engine heads are tested for a few times. In addition to that, to understand the effects of the surface roughness a plastic prototype is produced with a rapid prototyping machine for one of the considered intake port geometries as seen in the Fig. 5.

The roughness of the wall is an important factor for the natural vortex length, and therefore, the vortex end. An important effect is that it destabilizes the vortex in cyclones. If the roughness at the wall increases, the length of the vortex decreases. Hoffmann *et al.* (1995) reported that this was often caused by the effect given by an increase in dust loading (Peng *et al.*, 2005 & Qian and Zhang, 2005).

The effect of wall roughness influences the tangential velocity, efficiency, cyclone separation, and cyclone pressure drop for high inlet velocity (Kaya *et al.*, 2011). Qian and Zhang (2005) stated, "The natural vortex length decreases when the wall roughness increases".

During research and experiments of the surface roughness, Kaya *et al.* found that decreasing the tangential velocity and increasing the wall roughness in the cyclone led to an increase of the cut-size, in turn, a decrease in collection efficiency (Kaya *et al.*, 2011). The decrease in the inlet velocity also led to an increase in flow resistance and disappearance of the swirl. An excessive increase in the wall roughness led to an upward axial velocity increase in the core region. This is why the separation efficiency is exacerbated by increasing surface roughness. At high inlet velocities, an increase in wall roughness could also cause less pressure drop (Kaya *et al.*, 2011).

As it is reported in the different studies in the literature, surface roughness has significant effect on the vortex length, velocity and the swirl behavior of the flow.

3. NUMERICAL INVESTIGATION

In the present numerical study, steady state flow bench is considered and simulated. To create a virtual test bench, CFD based steady state simulations carried out with the commercial CFD software Converge. The numerical model solves the RANS equations with the finite volume approach. The main reason of using Converge is about the advantage on grid generation. Converge allows user to generate mesh according to domain characteristic in terms of velocity, temperature etc. during the simulation by adaptive mesh refinement (AMR) feature.

RNG k- ϵ turbulence model used for the simulations, which is recommended for the low Reynolds number flows and swirly flows, and gives more accurate results due to its additional term on the turbulent stress calculation.

The modelling details and simulation parameters explained below in the related sections.

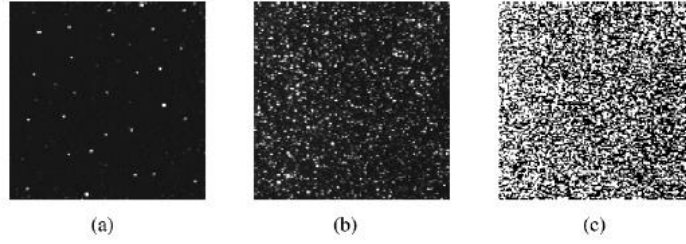


Fig. 4. Particle density and distribution (Raffel *et al.*, 2007).

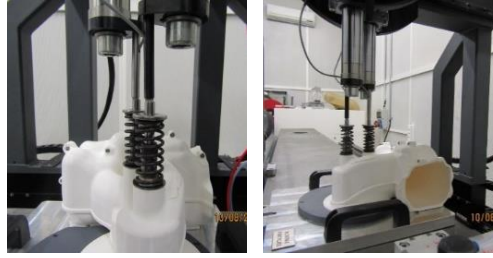


Fig. 5. Flow box design.

3.1 RNG k-ε Model

RNG k-ε model is used for the turbulence modelling in the simulations. RNG turbulent model gives more accurate results for the highly swirly flow at low Reynolds number. And it is commonly used turbulence model for the internal combustion engine applications.

RNG k-ε model requires additional transport equations to obtain the turbulent viscosity. There are two extra equations which RNG k-ε model needs. One of the equations is for the solution of the turbulent kinetic energy (k) as shown in Eq. (6) and the other equation is for the dissipation of turbulent kinetic energy (ε) as seen below in the Eq. (7) (Converge, version 2.3-Manual 2016).

$$\frac{\partial \rho k}{\partial t} + \frac{\partial \rho u_i k}{\partial x_i} = \tau_{ij} \frac{\partial u_i}{\partial x_j} + \frac{\partial}{\partial x_j} \left(\frac{\mu + \mu_t}{Pr_k} \frac{\partial k}{\partial x_j} \right) - \rho \varepsilon + \frac{c_s}{1.5} S_s \quad (6)$$

$$\frac{\partial \rho \varepsilon}{\partial t} + \frac{\partial (\rho u_i \varepsilon)}{\partial x_i} = \frac{\partial}{\partial x_j} \left(\frac{\mu + \mu_t}{Pr_\varepsilon} \frac{\partial \varepsilon}{\partial x_j} \right) + c_{\varepsilon 3} \rho \varepsilon \frac{\partial u_i}{\partial x_i} + \left(c_{\varepsilon 1} \frac{\partial u_i}{\partial x_j} \tau_{ij} - c_{\varepsilon 2} + c_s S_s \right) \frac{\varepsilon}{k} + S - \rho R \quad (7)$$

In the Eq. (7), S is a source term. R is equal to the zero for the standard k-ε model. On the other hand, RNG k-ε model has an additional definition for the R term as shown in the Eq. (8).

$$R = \frac{C_\mu \eta^3 \left(1 - \frac{\eta}{\eta_0} \right) \varepsilon^2}{(1 - \beta \eta^3) k} \quad (8)$$

η is calculated by:

$$\eta = \frac{k}{\varepsilon} |S_{ij}| \quad (9)$$

3.2 Geometrical Modelling

Simulation domain includes cylinder head, bore, piston, intake valves, and intake ports. To be able to simulate the exact test environment, part of the inlet manifold is included in the simulation domain as seen in the Fig. 6. A half sphere like plenum volume is specified as inlet to ensure accurate replication of the test environment. The diameter of the plenum equals to the four times the bore diameter. Exhaust valves are removed from the geometry and the area is closed. Piston is also removed since this study aims to simulate a steady state test bench.

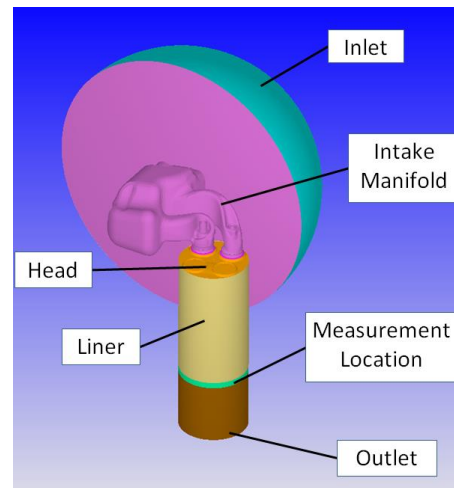


Fig. 6. Simulation domain.

Swirl measurement area shown in the Fig. 6 is located 1.75 times bore diameter away from the head (Converge Version 2.3- Flow bench QSG; Forte *et al.*, 2015).

For each valve lift, individual geometries are created and simulated until reaching flow convergence on the grid.

3.3 Grid Generation

Grid quality and resolution is prior for that kind of a simulation to be able predict the swirl correctly. It is important to determine flow velocity behavior precisely. Therefore, mesh is determined on the critical flow zones with a grid independence study. For the global mesh properties around the cylinder zone, adaptive mesh refinement feature is used in addition to local mesh refinements. This is how fluctuations are captured precisely. Then, grid independence study is carried out on the valve-seat interaction zone. Since the flow behavior is determined at this zone and it is important to have a high quality mesh especially for the smaller valve lifts. Results are evaluated in terms of change on the mass flow rate, swirl ratio and effects to the solution time and the mesh sizes are determined.

Base grid size is set as 4 mm. With the local mesh refinements, grid size is decreased down to 0.25 mm on the critical zones.

On the valve opening areas, mesh resolution is applied according to valve lift separately. If valve lift is higher than 6 mm, 0.5 mm sized mesh is generated with 3 layers and if lower than 6 mm, 0.25 mm sized mesh is generated with 4 layers to be able to calculate flow accurately for each valve lift starting from 1 mm to the highest.

On the liner and swirl measurement zones, mesh size is decreased to 0.5 mm by local refinements as seen in the Fig. 7. Second mesh refinement is applied to the outlet region which decreases mesh size to 1 mm.

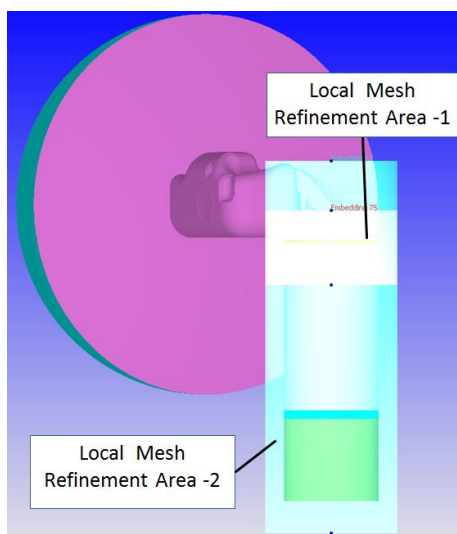


Fig. 7. Mesh refinement zones.

To be able to simulate other extraordinary flow movement, velocity AMR (Adaptive Mesh Refinement) is applied with the 0.5 mm mesh size and 1 m/s sub-grid criterion. This means for every 1 m/s velocity gradient, grid is being refined by the software automatically during the simulations.

Resulting mesh grid can be seen below in the Fig. 8 for the 11 mm valve lift.

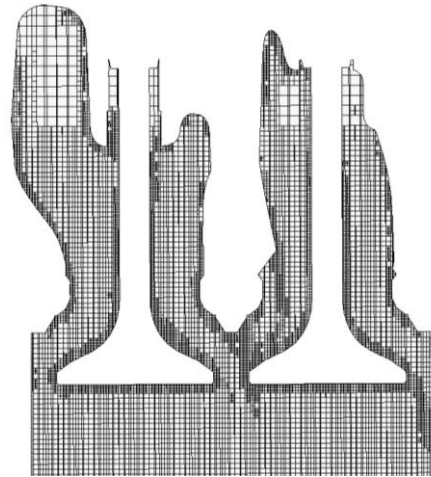


Fig. 8. Simulation grid.

3.4 Boundary Conditions

Fixed pressure boundary conditions are applied on both inlet and outlet boundaries for each valve lift. Inlet total pressure is set to zero Pa gauge pressure at 300K ambient temperature. On the other hand, outlet static pressure is set to 4900 Pa gauge vacuum pressure. Boundary conditions are gathered from the measurements.

3.5 Swirl Ratio Calculation

There are several calculation methods for swirl ratio in the literature, which are represented in different studies by different research groups. Moreover, some of these calculations are being used for the companies currently according to the test bench. In the present numerical study, FEV's swirl ratio calculation is considered, which is identical with the tests as explained in the Eq. (1).

The first step of the swirl prediction on the virtual environment is to calculate mass flow rate accurately. Since the swirl ratio definition has strong relationship with the mass flow rate. So that, mass flow rates are compared with the test results first, and 5 percent error is considered as acceptable.

Secondly, swirl ratio values are calculated by considering angular momentum flux (Nm) as torque value, which is measured at the 'Swirl Measurement Location' on Converge.

To avoid any numerical instabilities and the fluctuations on the mass flow rate and angular momentum flux calculations, average values are considered for these parameters. The last 5000 iterations are used for the averaging.

4. RESULTS

4.1 Comparison of Steady Flow Test Bench Measurements and CFD Results

The results are obtained for the steady flow bench for three different engine configurations and a flow box. Engine A and B configurations are also simulated by using the proposed CFD methodology. Engine C is used to understand the manufacturing problems' effects on the swirl ratio since significant discrepancy is observed due to the high manufacturing tolerances and problems during the measurements. Moreover, flow box is designed for the Engine-A geometry and used for the surface roughness investigations. The details of the engine structures are shown in the Table 1.

Table 1 Engine dimensions.

	A	B	C
Bore (mm)	115	130	80
Number of Cylinder	6	6	2
Number of Valves	4	4	2

Simulation results are compared with the measurements for the engine A and B to validate the methodology developed for the virtual flow bench. The first step of the validation is to compare the mass flow rates, since the swirl ratio has a strong dependency to the actual mass flow rate. Results are shown in Fig. 9.

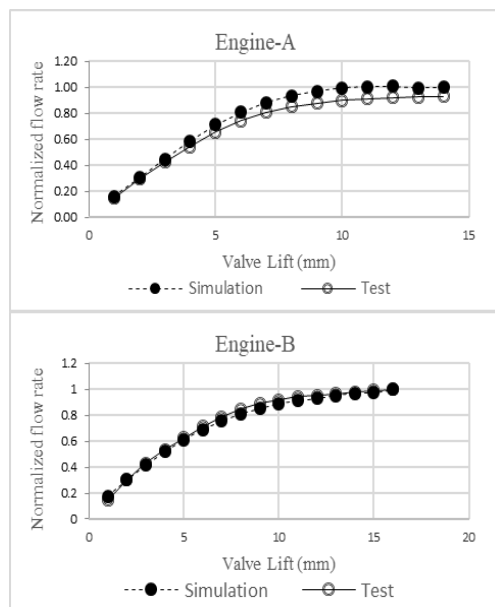


Fig. 9. Mass flow rate comparison.

In comparison with the measurements, especially on the higher valve lifts there are slight differences on the mass flow rate values. Mass flow rate is predicted higher in the CFD as expected due to the simplifications on the physical models and the difference on the surface quality. Since surface roughness is not specified on the CFD simulations. Regardless, the mass flow rate predictions are in the 5 percent range and accurate enough to determine the

swirl ratio.

The comparison for the swirl ratio calculated with CFD simulations and test measurements are shown in the Fig. 10 for Engine-A and Engine-B.

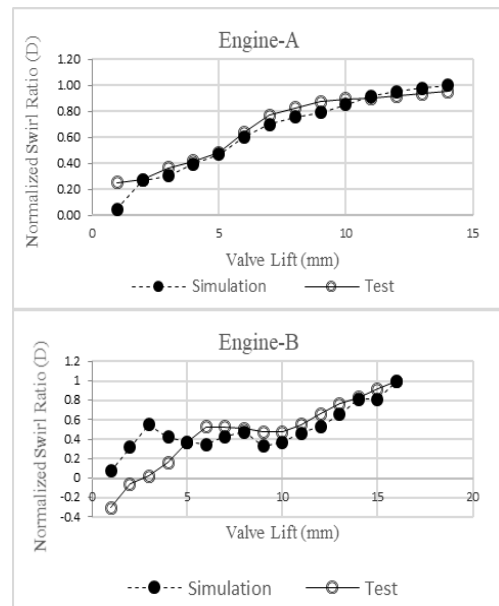


Fig. 10. Swirl ratio comparison.

Results showed a good agreement with the test data. Swirl ratio is predicted with a good accuracy by using the CFD simulations carried out in this study.

The only difference is observed on the Engine-B for the valve lifts smaller than 5 mm. Swirl ratio values for the very small valve lifts are calculated as negative in the tests. In order to identify the causes of the difference and the negative swirl ratio values, measurements and simulations are investigated in detail.

First, Mach number is calculated to understand whether flow regime is on the transonic region or not. Since the turbulence model isn't capable to capture the transonic flow. The velocity distribution on the critical valve section is shown in Fig. 11 for the 2 mm valve lift.

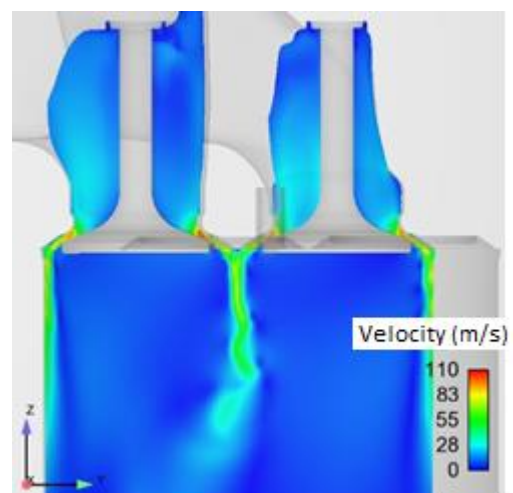


Fig. 11. Velocity distribution on the vertical section for 2 mm valve lift.

The Mach number for this case is around 0.35-0.5 and flow is in the limits of subsonic regime. In addition, the swirl behavior in such small valve lifts is not developed properly due to the low swirl ratio of the Engine-B as shown in the Fig. 12. And this results with discrepancies on the swirl ratio calculations.

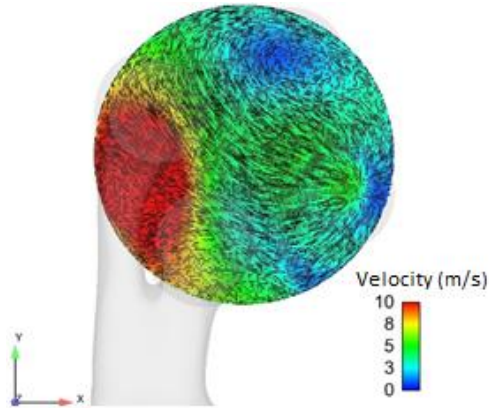


Fig. 12. Velocity distribution on the swirl measurement section for 2 mm valve lift.

Furthermore, the measurement system has higher tolerances in the smaller swirl ratios since the system is designed for the high swirl ratio measurements.

4.2 Comparison of PIV Measurements and CFD Results

PIV measurements are conducted for the Engine-A configuration for 11 mm valve lift on the section 125 mm below the deck face. Test results are shown in the Fig. 13 and CFD results are shown in the Fig. 14. Average flow regime is used instead of instantaneous scenes. Therefore, the PIV scene represents the average of 100 instant scenes.

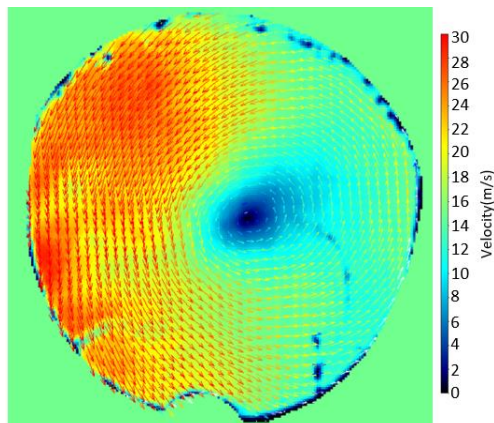


Fig. 13. PIV result for 11mm valve lift.

Even reflections are observed in the resulting scene for the PIV, vortex center can be clearly seen. High velocity region is located away from the intake valves.

CFD result has a good agreement with the PIV results in terms of the vortex location. On the other hand, even the high velocity flow regime is located on the same region with the PIV test, turbulence

model couldn't capture the exact velocity distribution and the flow behavior.

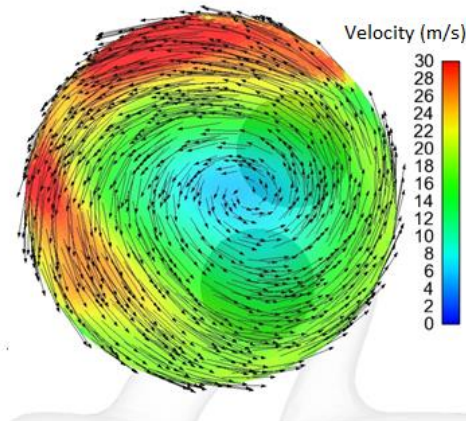


Fig. 14. CFD result for 11mm valve lift.

4.3 Effects of Surface Roughness

During the Engine-C swirl ratio measurements, significant discrepancy is observed between two cylinders as shown in the Fig. 15. Measurements are repeated for three times and resulted with the same swirl ratio behavior.

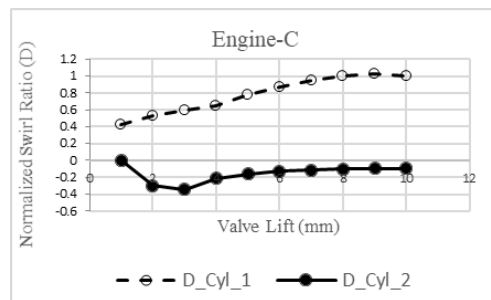


Fig. 15. Engine-C swirl ratio over valve lift.

Even one of the cylinders has swirl ratio as expected in positive numbers for each valve lifts, second cylinder has negative swirl ratio values for each valve lifts, which indicates that the swirling flow occurs on the opposite directions in cylinder. To understand the reason of the discrepancy between two cylinders of the Engine-C, endoscopic visualization technique is used to understand the surface quality. Endoscopic camera observations are shown in Fig. 16.

Endoscopic diagnostic results pointed out that the surface roughness differs cylinder to cylinder. The most important observation is that there is a tilt problem on the intake valve of the second cylinder. Valve is not mounted properly in the center axis and as a result of that valve vibrates with the flow forces. This leads to a very different flow behavior inside the cylinder and negative swirl ratio values. This observation shows the significance of the manufacturing tolerances and accuracy considering the significant effect on the swirl ratio values over valve lift.



Fig. 16. Endoscopic camera scenes for Engine-C.

In addition to the endoscopic investigation for the Engine-C to understand the surface roughness and the manufacturing tolerances, a plastic prototype is produced for the Engine-A. Even there is no problem on the Engine-A cylinder head in terms of surface roughness or valve tilt, prototype has almost perfectly smoothed surface. In comparison with cast cylinder head, flow box reaches higher flow coefficient values as shown in the Fig. 17.

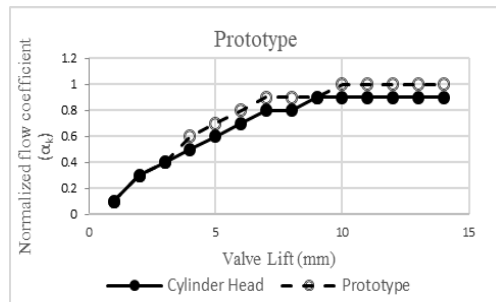


Fig. 17. Flow coefficient comparison of flow box and Engine-A.

On the other hand, swirl ratio distribution over the valve lift changes with the flow box as shown in the Fig. 18.

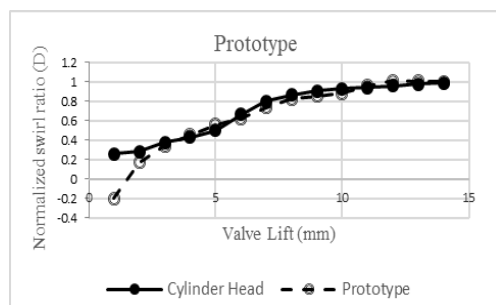


Fig. 18. Swirl ratio comparison of flow box and Engine-A.

For the 1 mm valve lift, flow box results with negative swirl number due to leakage problems.

Since the spring constant used for the flow box is smaller than the exact spring constant used in the production because of the durability considerations for the plastic prototype.

5. CONCLUSION

In the present study, numerical and experimental investigation techniques are used to characterize flow field in diesel engine combustion chamber. Three different engine structures are used for the investigations; Engine-A, Engine-B and Engine-C. Moreover, a plastic prototype is produced by using rapid prototyping device and used for the surface roughness investigations and PIV measurements.

A validated CFD model is built to analyze in cylinder flow behavior for modern diesel engines. Predictions showed a good agreement with the swirl ratio measurement results for Engine-A and Engine-B, which used to validate the CFD simulations. Mass flow rate values are predicted within 5 percent error and swirl ratio values are predicted within 10 percent error.

Additionally, PIV measurements are conducted for the Engine-A and results are discussed in detailed. It is observed that, even the current turbulence model is capable to predict the average flow behavior, which is digitized with swirl ratio accurately; velocity distribution is not captured precisely. LES (Large Eddy Simulation) can be used to observe the flow distribution precisely, in the further studies.

On the other hand, surface roughness effect and effects of manufacturing problems are investigated and discussed. Results showed the importance of the manufacturing problems for the engines. Since there is a significant impact on the swirl ratio, which is the key parameter for the combustion efficiency in cylinder, as observed in the Engine-C measurements. Moreover, flow box measurements are pointed out that, the flow coefficient and the swirl ratio values can change due to the surface roughness effects.

As a conclusion, the present validated numerical methodology gives chance to design for the first time

true and proper intake port geometries for the considered combustion chamber. Moreover, by using the numerical method, further optimization studies can be conducted by using recently developed optimization algorithms such as, genetic algorithm or design of experiment. In addition, the plastic prototype approach introduced in this study can be used to validate the design alternatives before having a production cylinder head or metal prototype.

ACKNOWLEDGEMENTS

The authors would like to acknowledge Aydın Ayyıldız for his assistance with testing performance in Ford Otosan.

REFERENCES

- Bhushan, B. (1996), *Tribology and Mechanics of Magnetic Storage Devices*. 2nd edition, Springer, New York.
- Bhushan, B. (1999a). *Principles and Applications of Tribology*. Wiley, New York.
- Bhushan, B. (1999b). *Handbook of Micro/Nanotribology*. 2nd edition, CRC, Boca Raton.
- CONVERGE (Version 2.3) Computer software (2016). Flowbench_QSG, *Convergent Science, Inc.*
- CONVERGE (Version 2.3) Computer software (2016). Manual, *Convergent Science, Inc.*
- Costa, M., G. Bianchi, C. Forte and G. Cazzoli (2014). A numerical methodology for the multi-objective optimization of the DI diesel engine combustion. *Energy Procedia* 45, 711-720.
- EUROPARL (2009). *The European Parliament and the Council*, R. (EC).
- Forte, C., C. Catellani, G. Cazzoli, G. M. Bianchi, S. Falfari, F. Brusiani, A. Verzè and S. Saracino (2015). Numerical evaluation of the applicability of steady test bench swirl ratios to diesel engine dynamic conditions. *Energy Procedia* 81, 732-741.
- Gan, X., D. Yao, F. Wu, J. Dai, L. Wei and X. Li (2016). Modeling and simulation of urea-water-solution droplet evaporation and thermolysis processes for SCR systems, *Chinese Journal of Chemical Engineering* 1065-1073.
- Haktan, K. Z., Kumlutas D. and O. Ozer (2012). Particle image velocimetry method (PIV): Split air conditioner indoor unit. *Journal of Sogutma Dnyasi* (56).
- Han, T. Q., S. J. Wu and W. Li (2007). Design and Experimental Evaluation of Inlet Port of Four-Valve Cylinder Head of a Heavy Vehicle Diesel Engine. *Chinese Internal Combustion Engine Engineering* 28(2), 47-50.
- Heywood, J. (1988). *Internal Combustion Engine Fundamentals*. Massachusetts, USA: McGraw-Hill Inc.
- Hirata, K., N. Masaki, H. Ueno and H. Akagawa (2005). Development of Urea-SCR System for a Heavy-Duty Commercial Vehicles. *SAE Technical Paper Vols.* 2005-01-1860.
- Hoffmann, A. C., R. de Jonge, H. Arends and C. Hanrats (1995, September). Evidence of the 'natural vortex length' and its effect on the separation efficiency of gas cyclones. *Filtration & Separation* 32, 8 (9 1995), 799-804.
- Kamimoto, T. and H. Kobayashi (1991). Combustion processes in diesel engines. *Progress in Energy and Combustion Science* 17, 163-189.
- Kaya, F., I. Karagoz and A. Avci (2011, August). Effects of surface roughness on the performance of tangential inlet cyclone separators. *Aerosol Science and Technology* 988-995.
- Kim, Y., Y. Han and K. Lee (2014). A study on the effects of the intake port configurations on the swirl flow generated in a small DI diesel engine. *Journal of Thermal Science* 23(3), 297-306.
- Krishnan T. T. A. R. (2005, January). *Diesel Technical Report*. [Online]. Available: <https://www.dieselnet.com/papers/0501krishnan>.
- Peng, W., A. C. Hoffmann, H. W. A. Dries, M. A. Regelink and L. E. Stein (2005). Experimental study of the vortex end in centrifugal separators: The nature of the vortex end. *Chemical Engineering Science* 60, 24 (12), 6919-6928.
- Qian, F. and M. Zhang (2005). Study of the natural vortex length of a cyclone with response surface methodology. *Computers & Chemical Engineering* 29, 10.
- Raffel, M., C. E. Willert, S. T. Wereley and J. Kompenhans (2007). *Particle Image Velocimetry, A Practical Guide*, Springer-Verlag Berlin Heidelberg.
- Roy, O. and L. Penven (1998). Compression of a turbulent vortex flow. *International Journal of Heat and Fluid Flow* 19, 533-540.
- Steger, J. (1995). Advances in Emission Control Technology. in *Emission Control and Catalytic Combustion TOPTEC*.
- Stone, C. and N. Ladommatos (1992). The Measurement and Analysis of Swirl in Steady Flow. *SAE Technical Paper* 921642.
- Sun, J. , D. Yates and D. Winterbone (1996). Measurement of the flow field in a diesel engine combustion chamber after combustion by cross-correlation of high-speed photographs. *Experiments in Fluids* 20, 335-345.
- Thomas, T. R. (1999). *Rough Surfaces*, 2nd ed., Imperial College Press, London, U.K.
- Tippelmann, G. A. (1977). New Method of Investigation of Swirl Ports. *SAE paper No.* 770404.

C. Demirkesen *et al.* / *JAFM*, Vol. 13, No. 2, pp. 537-547, 2020.

Uzkan, T., C. Borgnakke and T. Morel (1983).
Characterization of Flow Produced by a High-
Swirl Inlet Port. *SAE* paper No. 830266.

Weltens, H., H. Bressler, F. Terres, H. Neumaier and
D. Rammosewr (1993). Optimisation of

catalytic converter gas flow distribution by
CFD prediction. *SAE* Paper 930780.

Whitehouse, D. J. (1994). *Handbook of Surface
Metrology*. Institute of Physics Publishing,
Bristol, U.K.